Accumulative effects in the coherence of three-level atoms excited by femtosecond-laser frequency combs

D. Felinto, L. H. Acioli, and S. S. Vianna*
Departamento de Física, Universidade Federal de Pernambuco, Recife-PE, 50670-901, Brazil
(Received 17 January 2004; published 12 October 2004)

We investigate coherent accumulation processes in three-level atoms excited by a train of ultrashort pulses in the case where the atomic relaxation times are greater than the laser repetition period. In this situation the resonances of the laser field with the atomic system are determined by the laser frequency comb rather than by the spectrum of a single pulse. Using the density matrix formalism, we develop a perturbative theory that is valid for arbitrary pulse shapes. The excitation of a Doppler-broadened atomic vapor by hyperbolic-secant pulses and 0π pulses is analyzed. It is shown that pulse shape has a great influence on the accumulation process and can change the spectral periodicity of the pattern impressed on the Doppler profile of the medium due to the two-photon absorption process. The effect of interpulse phases is also investigated, and we show that the atomic populations can vary by more than one order of magnitude with small variations of the laser repetition rate, while being insensitive to variations of the laser offset. Finally, the theory is adapted for the temporal-coherent-control technique, and its results are compared with previously reported experimental data.

DOI: 10.1103/PhysRevA.70.043403 PACS number(s): 32.80.Qk, 42.50.Gy, 42.50.Md

I. INTRODUCTION

The field of coherent control of quantum systems comprises a set of techniques designed for finding the pulse shape that maximizes one of the possible outcomes of the system at the expense of the others. The desired outcome varies from one system to another: in atoms or molecules, for example, the goal is usually to excite a specific internal state, while for chemical reactions it is to control the ratio of competing products of a reaction [1,2]. One of the simplest techniques employed in coherent control is known as temporal coherent control where combinations of ultrashort pulses with variable relative delays are used to excite the sample [3]. In these configurations the pulses usually have the same shape, and control is achieved by scanning their relative delay. Another important technique is known as optimal control [4], which is accomplished by the shaping amplitude and phase of the spectral components of individual pulses. This is commonly done with the aid of a programmable liquid-crystal light modulator [5], which allows one to modify the pulse spectrum in a very general manner. Some pulse shapes, however, are better produced by simply propagating the pulses from the laser through an atomic vapor [6]. This is the case, for example, for zero-area pulses (0π pulses) [6,7]. The main characteristic of the action of 0π pulses on an atomic transition is that they leave no population on the higher-lying state on their passage through the sample, even though they have finite energy.

The coherent control techniques are habitually designed for the excitation of the system by single pulses from the laser. However, it was recently shown that the accumulation of excitation in the sample with a sequence of laser pulses coming from passively mode-locked femtosecond lasers can have great influence on a temporal-coherent-control signal from a rubidium vapor [8]. Accumulation occurs when the relaxation times of the medium are longer than the laser pulse repetition period T_R, which is determined by the round-trip time of the pulse within the laser cavity. For most femtosecond laser oscillators $T_R \approx 1-10$ ns, and accumulation should therefore be present for atoms with relaxation times greater than 10 ns, when excited by such pulse trains. It is therefore important to discuss a generalization of the coherent-control schemes considering the interaction of a quantum system with the whole train of pulses coming out of the laser. In the frequency domain, the periodic pulse train of a mode-locked laser can be described as a comb of equidistant modes. This frequency comb has received great attention in the last years in connection with its application in metrology at optical frequencies [9–11]. For atomic systems, the frequency comb determines the resonances between the atom and laser field in the case when the atomic coherence survives between two consecutive laser pulses [12]. In this situation, a *coherent accumulation* of excitation occurs in the sample, and the final atomic populations are determined by constructive or destructive interferences between the coherences excited by the sequence of pulses from the laser [12]. The result of this process can be understood as a temporal analog of a multiple-slit interferometer experiment [13].

An important application of these ideas has been the use of frequency combs in spectroscopic measurements with a resolution that is much better than the one determined by the Fourier transform from a single pulse in the train. Basically, the resolution is now given by the width of the comb's teeth in the frequency domain, which can be extremely small. This effect has been explored since 1978, when the feasibility of Doppler-free two-photon spectroscopy with multiple light pulses was demonstrated [14]. One of the best examples of the application of pulse trains for high-resolution spectroscopy was given by Snadden *et al.* in 1996 in the two-photon spectroscopy of laser-cooled rubidium [15].

In this paper we study the interaction of a train of femtosecond optical pulses with a sequential two-photon transition

*Electronic address: vianna@ufpe.br

in the case where the relaxation times of both atomic coherences and populations are greater than the pulse repetition period, resulting in an accumulative process during the pulse train. This problem has been investigated previously by Yoon *et al.* [16], where the emphasis was on metrological applications, and they considered a cold atom system, with no Doppler broadening. Differently from these works our emphasis is in coherent control. In particular, the procedure developed here is applied to the coherent control of the two-photon transition by pairs of optical pulses with variable delay τ. Despite the fact that we study atoms in a vapor cell excited by pairs of copropagating pulses, the theory presented here can also be applied to different systems, such as atoms in a magneto-optical trap. The paper is organized in the following manner: in Sec. II we present the optical Bloch equations for a three-level system interacting with a train of pulses delivered by a femtosecond laser and develop an efficient iterative numerical scheme to solve them. In Sec. III the iterative procedure is compared with direct numerical integration of the Bloch equations. Pulse shape effects are studied in detail for two different pulse envelopes, hyperbolic-secant and 0π pulses, interacting with a Doppler-broadened three-level system. In Sec. IV we discuss the role of the femtosecond pulse train parameters—the laser repetition period and interpulse phase difference—in the outcome of the sequential two-photon absorption process. In Sec. V previously reported results from coherent-control experiments of a three-level atom in cascade configuration are discussed in the light of the theory developed here, which takes into account coherent accumulation in these systems. Finally in Sec. VI the conclusions are presented.

II. ITERATIVE SOLUTION

We consider a three-level atom in a cascade configuration interacting with an electric field $E(t)$ from a laser pulse, with central frequency ω_L. The fundamental, intermediate, and upper levels are labeled $|1\rangle$, $|2\rangle$, and $|3\rangle$, respectively. The Hamiltonian of the system is given by $\hat{H}=\hat{H}_0+\hat{H}_{int}$, where $\hat{H}_0=\hbar\omega_{12}|2\rangle\langle 2|+\hbar\omega_{13}|3\rangle\langle 3|$ is the Hamiltonian of the free atom, with $\omega_{ij}=\omega_j-\omega_i$ and $\omega_1<\omega_2<\omega_3$. The coupling $\hat{H}_{int}$ describing the interaction between the atom and the electric field is

$$\hat{H}_{int}=-\mu_{12}E(t)|1\rangle\langle 2|-\mu_{23}E(t)|2\rangle\langle 3|+\text{H.c.}$$

We consider that the pulse bandwidth is large enough to cover both the ω_{12} and ω_{23} frequencies.

The Bloch equations describing the temporal evolution of the various elements ρ_{kl} of the atomic density matrix are given, in the rotating-wave approximation, by

$$\frac{\partial\rho_{33}}{\partial t}=\left(i\frac{\mu_{23}\mathcal{E}^*(t)}{\hbar}\sigma_{23}+\text{c.c.}\right)-\frac{\rho_{33}}{T_{33}}, \tag{1a}$$

$$\frac{\partial\rho_{22}}{\partial t}=\left(i\frac{\mu_{12}\mathcal{E}^*(t)}{\hbar}\sigma_{12}+\text{c.c.}\right)-\left(i\frac{\mu_{23}\mathcal{E}^*(t)}{\hbar}\sigma_{23}+\text{c.c.}\right)-\frac{\rho_{22}}{T_{22}}+\frac{\rho_{33}}{T_{33}}, \tag{1b}$$

$$\frac{\partial\sigma_{23}}{\partial t}=i\delta_{23}\sigma_{23}+i\frac{\mu_{23}\mathcal{E}(t)}{\hbar}(\rho_{33}-\rho_{22})+i\frac{\mu_{12}\mathcal{E}^*(t)}{\hbar}\sigma_{13}-\frac{\sigma_{23}}{T_{23}}, \tag{1c}$$

$$\frac{\partial\sigma_{12}}{\partial t}=i\delta_{12}\sigma_{12}+i\frac{\mu_{12}\mathcal{E}(t)}{\hbar}(2\rho_{22}+\rho_{33}-1)-i\frac{\mu_{23}\mathcal{E}^*(t)}{\hbar}\sigma_{13}-\frac{\sigma_{12}}{T_{12}}, \tag{1d}$$

$$\frac{\partial\sigma_{13}}{\partial t}=i\delta_{13}\sigma_{13}+i\frac{\mu_{12}\mathcal{E}(t)}{\hbar}\sigma_{23}-i\frac{\mu_{23}\mathcal{E}(t)}{\hbar}\sigma_{12}-\frac{\sigma_{13}}{T_{13}}, \tag{1e}$$

where T_{kl} is the relaxation time of the element kl of the density matrix, and $\mathcal{E}(t)=E(t)e^{-i\omega_L t}$ is the slowly varying envelope of the laser pulse. The population of level 1, ρ_{11}, was eliminated from Eqs. (1) by the normalization condition $\Sigma_j\rho_{jj}=1$. The coherences are represented in terms of their slowly varying envelopes: $\sigma_{12}=\rho_{12}e^{-i\omega_L t}$, $\sigma_{23}=\rho_{23}e^{-i\omega_L t}$, and $\sigma_{13}=\rho_{13}e^{-2i\omega_L t}$. The three detunings are defined relative to the laser's central frequency ω_L as

$$\delta_{12}=\omega_{12}-\omega_L, \tag{2a}$$

$$\delta_{23}=\omega_{23}-\omega_L, \tag{2b}$$

$$\delta_{13}=\omega_{13}-2\omega_L=\delta_{12}+\delta_{23}. \tag{2c}$$

A realistic model for a stabilized train of pulses coming out of the laser must take into account the existence of the phase difference between two consecutive pulses. Following Ref. [17] and considering T_R as the laser repetition period, we write this phase difference as $\Delta\Psi=\Phi_R+\omega_L T_R$, where Φ_R is the round-trip phase acquired by the laser within the cavity, and the second term comes from the group retardation in one cavity round trip. The electric field for the pulse train is therefore

$$E_T(t)=\sum_{n=0}^{\infty}E(t-nT_R)e^{in\Delta\Psi}=\left[\sum_{n=0}^{\infty}\mathcal{E}(t-nT_R)e^{in\Phi_R}\right]e^{i\omega_L t}=\mathcal{E}_T(t)e^{i\omega_L t}. \tag{3}$$

It is clear from Eq. (3) that we can apply the rotating-wave approximation for the whole train, where the slowly varying envelope is now $\mathcal{E}_T(t)$ instead of $\mathcal{E}(t)$. The frequency spectrum of $E_T(t)$ consists of a comb of laser modes separated by $\Delta\omega=2\pi/T_R$ and centered at ω_L. The frequency of the Nth mode of the laser is then given by ω_N, where

$$\omega_N=\omega_L+\frac{2\pi N}{T_R}+\frac{\Phi_R}{T_R}. \tag{4}$$

It is known that in order to characterize a certain mode of the laser spectrum only two parameters are necessary, which are the mode separation $\Delta\omega$ and the frequency offset, which is related to the phase ϕ_R [9]. In Eq. (4) the central frequency ω_L is an arbitrary parameter and is kept fixed in the calculations performed here.

In this article, we are interested in the situation where the atomic relaxation times are greater than the laser repetition period, and therefore both populations and coherences can accumulate in the sample. The atomic system is supposed to start at the ground state and later each subsequent pulse will find the atom in an arbitrary state. Numerical integration of the Bloch equations (1) can provide the temporal evolution of the system for any initial condition. However, such integration requires computational times that forbid its wide application to all problems treated in this article.

In order to circumvent this limitation, we have developed a numerical procedure that allows us to probe the temporal evolution of the system very efficiently. This calculation is based on an iterative solution in which the state of the system before the $(n+1)$th pulse from the laser is a function of the state before the nth pulse. The iterative expressions for the atomic state are obtained directly from the integration of Eqs. (1) under the three following approximations:

(i) The pulse is very short compared to all atomic relaxation times T_{kl}. Thus, we can write

$$\mathcal{E}(t)e^{t/T_{kl}} \approx \mathcal{E}(t).$$

(ii) The pulse is very short compared to the laser repetition period T_R.

(iii) $E(t)$ is weak enough to keep only the lowest-order term in the perturbative series.

Approximation (i) is easily satisfied by femtosecond pulses interacting with atomic systems, for which the relaxation times are on the order of 1 ns or greater. Approximation (ii) is also easily satisfied for most femtosecond lasers, even taking into account distortions introduced by the propagation of the pulse through a resonant medium, as discussed in the next section. Approximation (iii) is clearly the most restrictive one, as expected for a perturbative theory.

Let ρ_{ij}^n be the element ij of the density matrix describing the atomic state before the nth pulse. If $\mathcal{E}_n(t)$ is the envelope of the nth pulse, the state before the $(n+1)$th pulse is then given by

$$\rho_{33}^{n+1} = e^{-T_R/T_{33}}\{|I_3|^2 + (1-|I_2|^2)\rho_{33}^n + |I_2|^2\rho_{22}^n - (I_2^*\sigma_{23}^n + \text{c.c.}) + (I_3^*\sigma_{13}^n + \text{c.c.}) - (I_2 I_3^*\sigma_{12}^n + \text{c.c.})\}, \tag{5a}$$

$$\rho_{22}^{n+1} = e^{-T_R/T_{22}}\{|I_1|^2 + (1-2|I_1|^2 - |I_2|^2 + I_6|I_2|^2)\rho_{22}^n - [(I_1^* I_2^* - I_6 I_3^*)\sigma_{13}^n + \text{c.c.}] + (|I_2|^2 - |I_1|^2 - I_6|I_2|^2 + I_6)\rho_{33}^n - (I_1^*\sigma_{12}^n + \text{c.c.}) + [(I_2^* - I_6 I_2^*)\sigma_{23}^n + \text{c.c.}]\}, \tag{5b}$$

$$\sigma_{23}^{n+1} = e^{i\delta_{23}T_R - T_R/T_{23}}\{-I_1^* I_3 + (1 - I_4^* - 2I_5)\sigma_{23}^n - I_2^2\sigma_{32}^n - I_1^*\sigma_{13}^n + I_2\rho_{33}^n - I_2\rho_{22}^n + I_1^* I_2\sigma_{12}^n + I_3\sigma_{21}^n\}, \tag{5c}$$

$$\sigma_{12}^{n+1} = e^{i\delta_{12}T_R - T_R/T_{12}}\{-I_1 + (1 - I_5^* - 2I_4)\sigma_{12}^n - I_1^2\sigma_{21}^n + I_2^*\sigma_{13}^n + 2I_1\rho_{22}^n + I_1\rho_{33}^n + I_1 I_2^*\sigma_{23}^n + (I_1 I_2 - I_3)\sigma_{32}^n\}, \tag{5d}$$

$$\sigma_{13}^{n+1} = e^{i\delta_{13}T_R - T_R/T_{13}}\{I_3 + (1 - I_4 - I_5)\sigma_{13}^n + I_1\sigma_{23}^n - I_2\sigma_{12}^n + (I_1 I_2 - 2I_3)\rho_{33}^n - (I_1 I_2 + I_3)\rho_{22}^n\}, \tag{5e}$$

where

$$I_1 = i\frac{\mu_{12}}{\hbar}\int_{-\infty}^{\infty} dt'\,\mathcal{E}_n(t')e^{-i\delta_{12}t'} = i\frac{\mu_{12}}{\hbar}\tilde{E}(\omega_{12}), \tag{6a}$$

$$I_2 = i\frac{\mu_{23}}{\hbar}\int_{-\infty}^{\infty} dt'\,\mathcal{E}_n(t')e^{-i\delta_{23}t'} = i\frac{\mu_{23}}{\hbar}\tilde{E}(\omega_{23}), \tag{6b}$$

$$I_3 = -\frac{\mu_{12}\mu_{23}}{\hbar^2}\int_{-\infty}^{\infty} dt'\,\mathcal{E}_n(t')e^{-i\delta_{23}t'}\int_{-\infty}^{t'} dt''\mathcal{E}_n(t'')e^{-i\delta_{12}t''}, \tag{6c}$$

$$I_4 = \frac{\mu_{12}^2}{\hbar^2}\int_{-\infty}^{\infty} dt'\,\mathcal{E}_n(t')e^{-i\delta_{12}t'}\int_{-\infty}^{t'} dt''\mathcal{E}_n^*(t'')e^{i\delta_{12}t''}, \tag{6d}$$

$$I_5 = \frac{\mu_{23}^2}{\hbar^2}\int_{-\infty}^{\infty} dt'\,\mathcal{E}_n(t')e^{-i\delta_{23}t'}\int_{-\infty}^{t'} dt''\mathcal{E}_n^*(t'')e^{i\delta_{23}t''}, \tag{6e}$$

$$I_6 = \frac{1}{T_{33}}\int_0^{T_R} dt'\,\exp\left(\frac{t'}{T_{22}} - \frac{t'}{T_{33}}\right). \tag{6f}$$

The set (5) of equations forms the basis for all subsequent discussions. Note that I_1 and I_2 are proportional to the Fourier transform of the pulse at the frequencies of the first and second transitions, respectively. These factors are thus related to the processes of absorption and stimulated emission on these transitions. The factor I_3 is related to two-photon processes connecting levels 1 and 3. The terms I_4 and I_5 represent second-order contributions to the one-photon transitions and are related to absorption saturation and stimulated emission of the first and second transitions, respectively. I_6 is related to the variation of the population in level 2 caused by spontaneous emission from level 3 to level 2 and from level 2 to level 1.

III. PULSE-SHAPE EFFECTS

If the laser repetition period is smaller than the relaxation times of the system, the atoms never fully relax between

consecutive pulses from the laser. In this situation, the medium accumulates excitation in the form of coherence and population in the excited states as the sequence of pulses arrives. In order to treat this problem, the first step was deducing Eqs. (5), which describe the interaction of individual pulses from the train with the atom in an arbitrary initial state. The next step is to employ these expressions to determine the temporal evolution of the system with a sequence of pulses. This is done by the successive application of Eqs. (5) to a certain initial state. Since this set of equations provides the state of the system before the arrival of the next pulse, its successive application results in the description of the desired temporal evolution over the whole pulse train.

In Secs. III A and III B we investigate the excitation of a sequential transition by trains of hyperbolic-secant pulses and 0π pulses, respectively. In order to make a connection with previously reported experimental data [8,18], the values of the parameters used in the calculations correspond to the excitation of the sequential transition $5S \rightarrow 5P_{3/2} \rightarrow 5D$ in a rubidium vapor by a Ti:sapphire laser femtosecond. Thus the laser is tuned to 778 nm, and we consider pulses of temporal width $T_p = 140$ fs, with repetition period $T_R = 13$ ns. The levels $5S$, $5P_{3/2}$, and $5D$ are labeled $|1\rangle$, $|2\rangle$, and $|3\rangle$, respectively. The lifetimes of levels $|2\rangle$ and $|3\rangle$ are $T_{22} = 26.7$ ns and $T_{33} = 241$ ns [19]. For the homogeneous broadening, we consider only radiative processes and take $T_{12} = 2T_{22} = 53.4$ ns, $T_{13} = 2T_{33} = 482$ ns, and $T_{23} = [(2T_{22})^{-1} + (2T_{33})^{-1}]^{-1} = 48.1$ ns. We also consider an inhomogeneous Doppler broadening of linewidth $\delta_D/2\pi = 0.2$ GHz. The ratio between the dipole moments of the first and second transitions is $\mu_{23}/\mu_{12} \simeq 0.2$ [20]. In both Secs. III A and III B, the magnitude of the electrical field is such that $\mu_{12}\mathcal{E}_0/\hbar = 0.2$ THz, where $\mathcal{E}_0$ is the peak value of $\mathcal{E}(t)$. Also, from these parameters, we have $I_6(T_R) \simeq 0.07$.

In what follows δ_{ij}^0 represents the detuning, relative to the laser's central frequency ω_L, for a group of atoms at rest in the laboratory reference frame. In this case the detunings for an arbitrary group of atoms in the Doppler profile can be written as $\delta_{12} = \delta_{12}^0 - \delta$, $\delta_{23} = \delta_{23}^0 - \delta$, and $\delta_{13} = \delta_{13}^0 - 2\delta$, where δ is the Doppler detuning with respect to the one-photon transitions and we neglect the difference (on the order of $10^{-3}\delta$) in the Doppler detunings of the first and second transitions. For simplicity, we also consider $\delta_{13}^0 = 0$, which means that the laser central frequency is resonant by two photons for the group of atoms at rest in the laboratory frame. The detunings can then be written as

$$\delta_{12} = -\Delta - \delta, \tag{7a}$$

$$\delta_{23} = \Delta - \delta, \tag{7b}$$

$$\delta_{13} = -2\delta, \tag{7c}$$

where $\Delta = (\omega_{23} - \omega_{12})/2 = 2\pi \times 1.056$ THz for the rubidium transition we are considering. Note that the detuning δ labels the different groups of atoms within the Doppler profile.

A. Hyperbolic-secant pulses

In order to clarify how Eqs. (5) are applied to our problem, in Fig. 1 we compare results from a direct numerical integration of Eqs. (1) with those obtained from Eqs. (5). We consider a train of hyperbolic-secant pulses interacting with an atom initially in the ground state. Equations (1) were integrated for one arbitrary group of atoms within the Doppler profile using a standard fourth-order Runge-Kutta method with adaptative step size [21]. The results for $\rho_{22}(t)$ and $\rho_{33}(t)$ are plotted as the solid lines in Fig. 1(a). Equations (5) are applied to the state of the system before an arbitrary pulse of the train and provide the state just before the next pulse arrives. The results for ρ_{22} and ρ_{33}, after successive applications of Eqs. (5) to the initial state, are given by open circles in Figs. 1(a) and 1(b). As the lifetime of levels 2 and 3 are very different, their transient behavior also occurs in different time scales as shown in pictures (a) and (b) of Fig. 1. As an estimate for the efficiency of this iterative solution we notice that in a computer where the numerical integration of Eqs. (1) takes about 1.5 h, the calculation based in Eqs. (5) takes less than 10 s. In order to obtain the behavior over the whole Doppler profile the first method becomes too slow to implement.

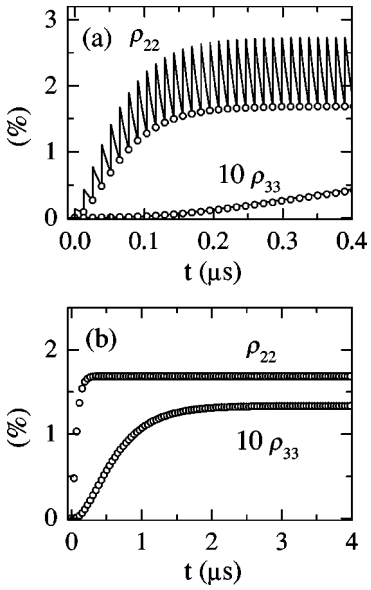

FIG. 1. Temporal evolution of the populations ρ_{22} and ρ_{33} starting at the fundamental state, interacting with a train of hyperbolic-secant pulses. In picture (a) the solid lines come from direct numerical integration of Eqs. (1). The (a) and (b) frames show different scales of the same temporal evolution where the open circles come from successive applications of Eqs. (5). In (b) we plot one open circle out of three to improve visualization. We set $\Phi_R = 0$ and $\delta = 0$.

The results for $t > 2$ μs in Fig. 1(b) determine the value of the stationary state ρ^f for coherent accumulation. All the density matrix elements reach a stationary value in the same way and they are numerically independent of the initial condition. This behavior indicates that the final state of the system only depends on a self-consistent condition that relates ρ^{n+1} to ρ^n. This condition, however, cannot be simply $\rho^{n+1} = \rho^n$, as in incoherent accumulation theories [8,22], since there is a phase difference Φ_R between two pulses. For the set (5) of equations, the final self-consistent expression for the density

matrix is quite cumbersome to write down due to the many variables involved. We have preferred to follow a more direct approach: the expression for ρ^{n+1} is iterated, beginning in the initial state ρ^0, until it reaches the stationary state we wish to calculate.

In Fig. 1 we have considered $\Phi_R=0$, $T_R=13$ ns, and the group of atoms with $\delta=0$. If the conditions $\delta_{12}T_R=2\pi N_{12}$ and $\delta_{23}T_R=2\pi N_{23}$ are satisfied with N_{12} and N_{23} integers, then we have an enhancement factor of order of 13 as compared to the final result ρ_{22} due to a single pulse, given by the first maximum of solid line in Fig. 1. For ρ_{33} this enhancement factor is of order of 35 000. These values are much larger than the incoherent enhancement factors expected from the theories that consider only population accumulation [8,22]. For the values of T_{22} and T_{33} used here, these incoherent factors are $\gamma_{22}=1.6$ and $\gamma_{33}=18$ for the populations ρ_{22} and ρ_{33}, respectively. Such large enhancement factors result from the constructive interference between the coherences excited by the sequence of pulses. This can be understood considering that the phases acquired by the coherences with the succession of pulses are analogous to the phases that result in the interference in a multiple-slit experiment [13,23]. Based on Eqs. (5) and for the three-level system that we study here, the conditions for constructive interference, when $\Phi_R=0$, are

$$\delta_{12}T_R = -\Delta T_R - \delta T_R = 2N_{12}\pi, \tag{8a}$$

$$\delta_{23}T_R = \Delta T_R - \delta T_R = 2N_{23}\pi, \tag{8b}$$

$$\delta_{13}T_R = -2\delta T_R = 2N_{13}\pi, \tag{8c}$$

where N_{12}, N_{23}, and N_{13} are integers. Note that when the conditions (8a) and (8b) are satisfied, then Eq. (8c) is fulfilled. These conditions correspond to the case of Fig. 1.

For other groups of atoms, with $\delta\neq 0$, the conditions (8) are not necessarily fulfilled. In this case the picture is more complex and can lead to constructive or destructive interferences, depending on the value of δ. For a vapor of alkali atoms at room temperature, the inhomogeneous Doppler broadening is usually much larger than the homogeneous broadening. Since the different velocity groups correspond to different detunings, they are in different situations with respect to the accumulation process. This is illustrated in Fig. 2, where the solid lines give the variation of the final populations, (a) ρ_{22}^f and (b) ρ_{33}^f with the detuning δ, for the same parameters of Fig. 1 and weighted by the Doppler profile $\exp(-\delta^2/2\delta_D^2)$. Notice that $T_p \ll \delta_D^{-1}$, which guarantes the validity of Eqs. (5) for all δ considered here.

Using definition (4) for the frequency of the Nth mode of the laser the conditions (8) to obtain constructive interference for $\Phi_R=0$ can also be written as

$$\omega_{12} = \omega_{N_{12}}, \tag{9a}$$

$$\omega_{23} = \omega_{N_{23}}, \tag{9b}$$

$$\omega_{13} = \omega_{N_{12}} + \omega_{N_{23}}. \tag{9c}$$

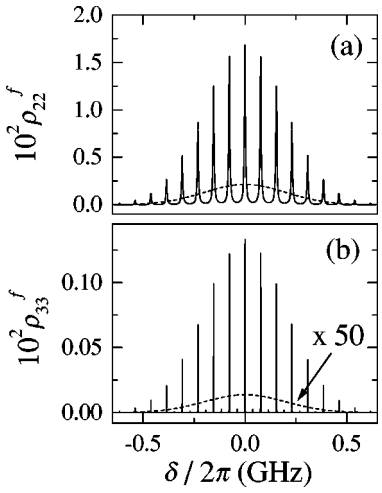

FIG. 2. The final populations (a) ρ_{22}^f and (b) ρ_{33}^f for the different atomic velocity groups in the inhomogeneous profile, excited by a train of hyperbolic-secant pulses. We consider $\Phi_R=0$ and $T_R=13$ ns. The dashed lines are obtained setting $T_{12}=T_{23}=T_{13}=1$ ns. In picture (b) the dashed line was multiplied by 50 to improve visualization.

These relations indicate that the peak structure in solid lines of Fig. 2 is a direct consequence of the resonance conditions. This observation is reinforced when considering $\Phi_R\neq 0$ in our analysis. In this case, the conditions for constructive interference are still the same as in Eqs. (9), so the inclusion of $\Phi_R\neq 0$ in Fig. 2 leads to a simple translation of the peaks by a quantity equal to $\Phi_R/2\pi T_R$. We notice that for a hyperbolic-secant pulse excitation the $1\rightarrow 2$ one-photon transition dominates the accumulation process. As a result, the two-photon Doppler profile shows a periodicity of $1/T_R$, instead of the expected $1/2T_R$.

In order to illustrate the transition from constructive to destructive interference as δ departs from a value satisfying conditions (9), we also plot in Fig. 2 the dashed lines which give the result for the same calculation, but with no accumulation in the coherence. This is accomplished by artificially setting $T_{12}=T_{23}=T_{13}=1$ ns into Eqs. (5). In this case, the approximation of short pulses (T_{22}, T_{33}, T_{12}, T_{23}, T_{13}, $T_R \gg T_p$) is still valid, but the coherences do not survive from one pulse to the next. The variation with δ of final populations, ρ_{22}^f and ρ_{33}^f, is now determined by the Doppler profile. In a crude manner it can be said that the part of the solid curve above the dashed line in Fig. 2 results from constructive interference, while the part below it results from destructive interference.

B. 0π pulses

One important characteristic of the set of equations (5) is that, once the short-pulse approximation is satisfied, then they are valid for any arbitrary pulse shape. This feature is useful in the coherent-control techniques which involve manipulation of the phase and amplitude of individual pulse shapes, which are crucial to determine the final atomic excitation. In this section we discuss the accumulative processes but now considering a 0π pulse, and our emphasis will be on

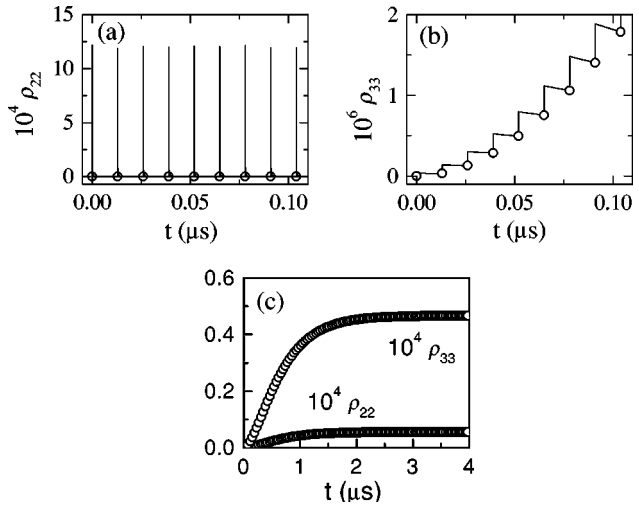

FIG. 3. Temporal evolution of the populations ρ_{22} and ρ_{33} starting at the fundamental state, interacting with a train of 0π pulses. The solid lines, in (a) and (b), come from direct numerical integration of Eqs. (1). The open circles come from successive applications of Eqs. (5). The pictures (a), (b), and (c) show different scales of the same temporal evolution. In (c), we plot one open circle out of three to improve visualization. We consider an optical density of $\alpha_0 l = 21$ and the other parameters are the same as in Fig. 1.

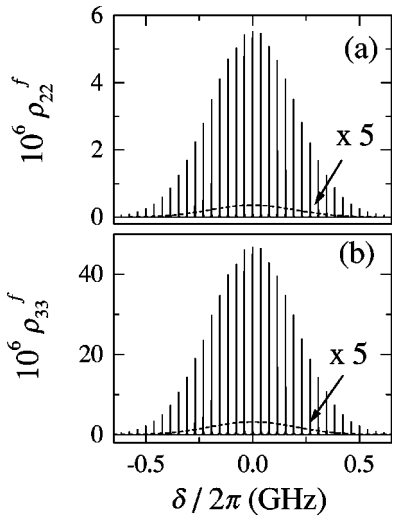

FIG. 4. The final populations (a) ρ_{22}^f and (b) ρ_{33}^f of the system excited by a train of 0π pulses for all group of atoms in the Doppler profile. All the parameters are the same of Fig. 3. The dashed lines are obtained setting $T_{12}=T_{23}=T_{13}=1$ ns and the results are multiplied by five to improve visualization.

the comparison with excitation by hyperbolic-secant pulses. We show that these two pulse shapes yield significant qualitative differences in the final result, indicating the importance of studying the details of a quantum system interacting with a train of pulses of arbitrarily shaped pulses.

In Fig. 3 are presented the results for the temporal evolution of the populations ρ_{22} and ρ_{33} interacting with a train of 0π pulses. This figure is completely analogous to Fig. 1: the solid lines in Figs. 3(a) and 3(b) are the results of numerical integration of Eqs. (1), whereas the open circles result from the successive applications of Eqs. (5) to the ground state. In Fig. 3(c) we show in a large temporal scale only the results from the successive applications of Eqs. (5) to the ground state. The parameters are the same used in Fig. 1, the only difference being the shape of the pulse.

One of main characteristics of a 0π pulse interacting with a two-level atom is a null excitation of the sample after the pulse passes through it [24]. In other words, it may be said that the trailing edge of the 0π pulse undoes the action of the leading edge, which can be verified after all the transients that happen during the interaction of the pulse with the atomic system are finished. For a cascaded three-level atom, a 0π pulse that is resonant with the intermediate transition also tends to cancel this transition. This explains the large transient in Fig. 3(a) and the negligible value for ρ_{22} before the next pulse arrives. However, when accumulation is taken into account, the intermediate level will be also excited by stimulated emission and spontaneous decay from the highest-lying level. This is the origin of the small plateau that appears in Fig. 3(c), which clearly evolves on the same time scale as the ρ_{33} population reaches its stationary state.

The contribution of the fast transient and the slowly evolving plateau to the temporal average of the final state of ρ_{22} can be calculated through the average of ρ_{22} in the excitation period (T_R). It is verified that the plateau corresponds to about $3/4$ of the final average population of level 2. We remark that the fast transient induced by the 0π pulse is a linear effect that has approximately the same shape over the whole pulse train. Therefore, the plateau is responsible for any variation of the ρ_{22} population due to accumulation effects. Based on these observations, in the following analysis we will only consider the contribution of the plateau, ρ_{22}^f, to the population of level 2.

The temporal behavior for the population ρ_{33} shown in Fig. 3 is very similar to that shown in Fig. 1. The enhancement factor of ρ_{33}^f relative to single-pulse excitation determined by the first maximum of the solid line in Fig. 3(b), but, however, is about 1300, much smaller than the value obtained for a hyperbolic-secant train of pulses. This is due to the fact that the sequential excitation pathway through level 2 is now negligible. Note also that the enhancement factor for the ρ_{22} population cannot be defined since the ρ_{22} excitation by a single 0π pulse vanishes. As can be seen in Figs. 3(c) and 3(b) the final stationary population ρ_{33}^f is larger than the final population of level 2, but the ρ_{33} excitation due to a single pulse is smaller than the average (fast) transient population of ρ_{22}. The population inversion in the second transition observed in Fig. 3 is therefore a consequence of the accumulation process.

The most significant characteristic of excitation by a train of 0π pulse appears in the analysis of the excitation of the system over the Doppler profile. Figure 4 shows the stationary density matrix elements ρ_{22}^f and ρ_{33}^f for all groups of atoms within the velocity distribution.

Compared to Fig. 2 which is obtained for a train of hyperbolic-secant pulses, it is noticeable that the periodicity of the peak structure for ρ_{22}^f is now $1/2T_R$ instead of $1/T_R$ as

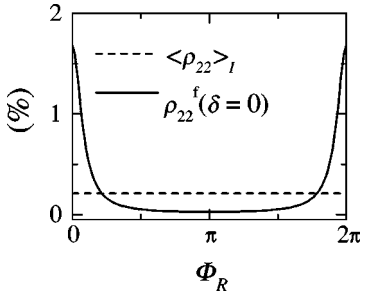

FIG. 5. Population in the intermediate state, ρ_{22}, for excitation with a hyperbolic-secant pulse, as a function of the interpulse phase Φ_R for one particular detuning, $\delta=0$ (solid line), and its value averaged over the Doppler profile, $\langle\rho_{22}\rangle_I$ (dashed line). In the last case, no variation with Φ_R is observed.

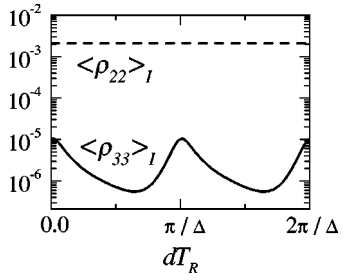

FIG. 6. Variation of the average populations $\langle\rho_{22}\rangle_I$ and $\langle\rho_{33}\rangle_I$ for excitation with a hyperbolic-secant pulse, as a function of the interpulse separation T_R: $\langle\rho_{22}\rangle_I$ is independent of T_R because some group of atoms is always found to be resonant by one-photon absorption, while $\langle\rho_{33}\rangle_I$ only satisfies all resonance conditions when $T_R = \pi N/\Delta$.

in Fig. 2. The ρ_{33}^f population shows the same periodicity as ρ_{22}^f. From conditions (8), we see that this periodicity indicates that the ρ_{13} resonant coherence drives the process, being responsible for the observed constructive and destructive interferences. This means that for excitation with a train of 0π pulse the two-photon transition dominates the accumulation process, contrary to what is predicted for hyperbolic-secant pulse excitation where the one-photon transition is dominant where the $1\rightarrow 2$ one-photon transition is dominant.

The effect of the 0π pulse in Eqs. (5) corresponds to $I_1 \approx 0$. In this case the nonzero source terms for ρ_{22} are related to the second transition. These terms originate from incoherent decay and stimulated emission from level 3 to level 2, which explains why ρ_{22}^f follows ρ_{33}^f. Note that the relation between coherent and incoherent excitation profiles (dashed line in Fig. 4) is also the same for ρ_{22}^f and ρ_{33}^f.

IV. PARAMETERS OF THE FREQUENCY COMB

The recent developments in the stabilization and measurement of the main parameters that characterize the pulse train delivered by femtosecond lasers have introduced a new paradigm in the area of metrology at optical frequencies [9–11]. In these lasers typically 10^5–10^6 modes are excited, each one with a frequency given by Eqs. (4) [25]. As previuosly mentioned, the two main parameters that characterize the frequency comb are the mode separation and the frequency offset, which are directly related to T_R and Φ_R, respectively, and it is important to be able to control these two parameters independently [10]. In this section we investigate the dependence of the atomic populations of the three-level system on the parameters of frequency comb: interpulse phase difference Φ_R, pulse repetition period T_R, and hyperbolic-secant pulse shape. The atomic system is supposed to be Doppler broadened, but with a frequency spread that is much narrower than the pulse spectrum.

In what follows we refer to the resonance conditions Eqs. (9) obtained for $\Phi_R=0$. As previously noted, once these conditions are satisfied, if one makes $\Phi_R\neq 0$, this will correspond to a simple shift in the position of the peaks. For a particular group of atoms this phase change can have a dramatic effect. When considering a Doppler-broadened atomic system, the analysis becomes a bit more subtle. To find the total population in a determined atomic level one must now take an average over the inhomogeneously broadened profile. If the Doppler width is much larger than the mode spacing, $\delta_D \gg 2\pi/T_R$, the effect of varying Φ_R for this average value is therefore null, as may be seen from the dashed line in Fig. 5. This is so because if Eqs. (9) are satisfied for some group of atoms and a certain Φ_R, this will remain true for any other Φ_R.

On the other hand, varying the pulse repetition period T_R leads to changes of the mode spacing, therefore determining whether Eqs. (9) will be satisfied or not. To illustrate this point Fig. 6 depicts the variation of the average over the Doppler profile of the excited populations, $\langle\rho_{22}\rangle_I$ and $\langle\rho_{33}\rangle_I$ with dT_R, a small change in the pulse repetition period. It is clear that while $\langle\rho_{22}\rangle_I$ remains constant, $\langle\rho_{33}\rangle_I$ varies by more than an order of magnitude. This behavior may be understood by examining the resonance conditions (8), from which it can be verified that if $T_R=\pi N/\Delta$, then there will always be a group of atoms with a particular δ that satisfies all three conditions given in Eqs. (8). In this case $\langle\rho_{33}\rangle_I$ reaches its maximum value.

The population $\langle\rho_{22}\rangle_I$ is not sensitive to this problem, as it is governed by the coherence ρ_{12} for which the detuning δ_{12} always satisfies the resonance condition for some group of atoms. The population $\langle\rho_{33}\rangle_I$, however, depends crucially on both the $1\rightarrow 2$ and the $2\rightarrow 3$ transitions, and must therefore satisfy all three conditions in Eqs. (8). These conditions for $\langle\rho_{33}\rangle_I$ may be stated in a simpler manner, by noting that for the laser modes to match both atomic transitions, then the difference between the atomic frequencies, Δ, must be equal to some multiple of the mode spacing $2\pi/T_R$. For 0π pulses the above results do not apply because the sequential excitation mechanism which is responsible for the dependence of $\langle\rho_{33}\rangle_I$ with T_R is no longer effective.

The results from Figs. 5 and 6 may have an interesting application in the control of femtosecond lasers for optical metrology. The fact that the population $\langle\rho_{33}\rangle_I$ is sensitive to T_R but not to Φ_R indicates that monitoring this population provides an interesting procedure for independent control of T_R: variations in T_R produce measureable changes of $\langle\rho_{33}\rangle_I$, while this quantity is independent of Φ_R.

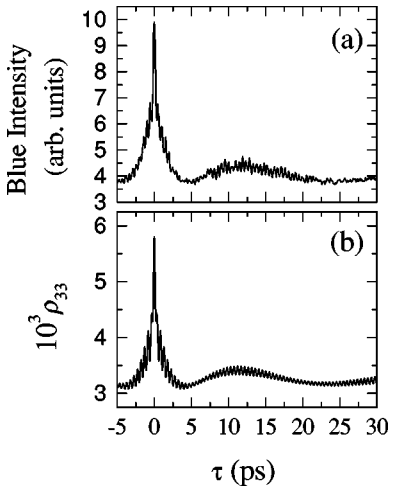

FIG. 7. (a) Variation of the blue fluorescence with relative delay, τ, between the pulse pairs for an atomic density of 7×10^{12} atoms/cm^3 and (b) numerical results for the variation of the population $\langle\rho_{33}\rangle_I$ as a function of τ, averaged over the Doppler profile.

V. TEMPORAL COHERENT CONTROL

In this section we apply the theory developed in the previous sections to the temporal coherent control of a three-level atom in a cascade configuration, including accumulation in both populations and coherences, and compare the results with previously reported experimental data in a rubidium vapor [18]. Although this is not the best testing ground for the theory developed here, as only the total population $\langle\rho_{33}\rangle_I$ (averaged over the Doppler profile) is measured, this can be considered as a first test. Also, as the relaxation times of both atomic coherences and populations involved in the experiment are greater than the pulse repetition period, the present theory is more adequate to describe the experimental results. In Ref. [18] a vapor of Rb atoms, enclosed in a 5-cm-long sealed cell, is excited by pairs of laser pulses tuned to $\lambda_L=778$ nm, which corresponds to the sequential $5S$-$5P_{3/2}$-$5D$ transition. The excitation source is a Ti:sapphire laser generating pulses of $\approx$100 fs and a repetition period of 13 ns. The measurement of $\langle\rho_{33}\rangle_I$ is performed indirectly by monitoring the fluorescence at 420 nm from the $6P_{3/2}$-$5S$ transition, which is proportional to the $5D$ population. The blue fluorescence is collected from the center of the cell in a right angle geometry. At the focal region the beam waist is $\approx$70 μm, and the average laser power is $\approx$100 mW. Once the pulse arrives at the center of the cell it has evolved into a 0π pulse, due to propagation in a resonant medium. In this case our theory predicts that $\langle\rho_{33}\rangle_I$ is insensitive to the phase Φ_R.

In order to describe this new situation, the first modification to be introduced in Eqs. (5) is to take into account that in Ref. [18] a train of copropagating pulse pairs is used instead of a train of single pulses. We consider pairs of pulses of equal shape, separated by a temporal delay τ, which is typically much shorter than the pulse period T_R. The envelope of the nth pulse pair is given by $\mathcal{E}_n(t)=\mathcal{E}_{n1}(t)+e^{(-i\omega_L\tau)}\mathcal{E}_{n1}(t-\tau)$. The integrals I_1-I_5 in Eqs. (5) now depend on τ and must be rewritten as

$$I_1 = i\frac{\mu_{12}}{\hbar}[1+e^{-i\omega_{12}\tau}]\tilde{E}_{n1}(\delta_{12}), \tag{10a}$$

$$I_2 = i\frac{\mu_{23}}{\hbar}[1+e^{-i\omega_{23}\tau}]\tilde{E}_{n1}(\delta_{23}), \tag{10b}$$

$$I_3 = F*(0)+e^{-i\omega_{12}\tau}F*(-\tau)+e^{-i\omega_{23}\tau}F*(\tau)+e^{-i\omega_{13}\tau}F*(0), \tag{10c}$$

$$I_4 = 2G(0)+e^{-i\omega_{12}\tau}G(-\tau)+e^{-i\omega_{12}\tau}G(\tau), \tag{10d}$$

$$I_5 = 2H(0)+e^{-i\omega_{23}\tau}H(-\tau)+e^{-i\omega_{23}\tau}H(\tau), \tag{10e}$$

where the functions $F(\tau)$, $G(\tau)$, and $H(\tau)$ are defined as

$$F(\tau) = -\frac{\mu_{12}\mu_{23}}{\hbar^2}\int_{-\infty}^{\infty}dt\int_{-\infty}^{t+\tau}dt'\,\mathcal{E}_{n1}^*(t)\mathcal{E}_{n1}^*(t')e^{i\delta_{23}t}e^{i\delta_{12}t'}, \tag{11a}$$

$$G(\tau) = \frac{\mu_{12}^2}{\hbar^2}\int_{-\infty}^{\infty}dt\int_{-\infty}^{t+\tau}dt'\,\mathcal{E}_{n1}(t)\mathcal{E}_{n1}^*(t')e^{-i\delta_{12}t}e^{i\delta_{12}t'}, \tag{11b}$$

$$H(\tau) = \frac{\mu_{23}^2}{\hbar^2}\int_{-\infty}^{\infty}dt\int_{-\infty}^{t+\tau}dt'\,\mathcal{E}_{n1}(t)\mathcal{E}_{n1}^*(t')e^{-i\delta_{23}t}e^{i\delta_{23}t'}. \tag{11c}$$

These functions all represent second-order processes in the applied fields but only $F(\tau)$ connects states 1, 2, and 3. Within the existing terms some present oscillations in the optical domain while others can be correlated to Ramsey-fringe-like experiments [3], occurring at time scales of $T_{opt}\approx 2\pi/\omega_L$ and $T_{quant}\approx 2\pi/2\omega_L$, respectively. We only consider the data taken at scan rates that are fast compared to the electronic aquisition times, in which case the interferometric effects are averaged to zero. Under this condition other (slower) oscillations occur at a period $T_{osc}=\pi/\Delta$, as shown in Fig. 7(a). These oscillations are related to stimulated emission in the transition $3\rightarrow 2$ [8,18] and are properly explained, considering only population accumulation [8]. The magnitudes of the final population in levels 2 and 3 predicted by incoherent accumulation theories, however, are significantly smaller than what is observed in the present theory.

As previously mentioned, this is only a first test of our method, and we are mainly interested in its sensitivity with the chosen fitting parameters, which are the pulse duration, pulse chirp, repetition period (T_R), and the phase (Φ_R). In this particular case, where the system is Doppler broadened and it interacts with a 0π pulse, it was important to observe that the qualitative form of the outcome of our simulations is sensitive to the frequency comb parameters only around the central peak.

To compare the numerical calculations with the experimental data, averages over 200 different values within each optical period are performed in the numerical calculations in order to simulate the effect of the fast scanning. For each value of the pulse separation τ, the iterative procedure was applied to obtain the final atomic coherences and popula-

tions. Averaging over the Doppler profile was also performed as it is the total population $\langle\rho_{33}\rangle_I$ that is experimentally observed.

For the frequency comb parameters we have taken Φ_R equal to zero, because of the insensitivity of the observed output to this parameter. Because the form of Eqs. (5), we conclude that the interval over which T_R should be adjusted is determined by $2\pi/\Delta \approx 1$ ps. Out of this range the results start to repeat themselves. The value of T_R which gives the best agreement with theory was found to be 13.0005 ns.

Another parameter that deserves attention is the frequency chirp of the laser. At the entrance of the cell the pulse is approximated by a hyperbolic-secant pulse which evolves into a 0π pulse due to propagation in the resonant medium. A quadratic phase in the frequency domain, defined by $\phi(\Omega)=aT_p^2\Omega^2/4$, is introduced in the pulse entering the cell, where a is an adimensional parameter that characterizes the chirp, Ω is the frequency measured from the center of the pulse spectrum, and T_p is the pulse duration. The introduction of chirp influences mainly the peak in the signal observed for $\tau \approx 0$.

In Fig. 7 are shown the comparison between (a) the experimental results and (b) the numerical results, and the main parameters used in the later are $\mu_{12}\mathcal{E}_0/\hbar = 1.4$ THz, $a=0.8$, and $T_R = 13.0005$ ns. It is important to recall that as only $\langle\rho_{33}\rangle_I$ is experimentally measured we cannot completely test the theory developed here. The overall behavior of the coherent-control experiment, however, has been satisfactorily reproduced. The main differences compared to the theory presented in Ref. [8] are observed around the central peak, where accumulation in the coherences ρ_{12} and ρ_{23} play an important role for the sequential excitation process.

It is important to note that for the numerical data presented in Fig. 7 we reached our computational limits: it has taken about 7 h to obtain these results. Full numerical integration of the Bloch equations would be out of question in this case.

VI. CONCLUSIONS

In this article we have presented a numerical iterative procedure to treat the problem of accumulation effects in both the population and coherences of an atomic system, for a sequential two-photon transition. The total excited populations in the intermediate and final states have been compared to incoherent accumulation theories, where dramatic differences are observed. We have used this procedure to analyze the effects of envelope pulse shapes for the outcome of the two-photon absorption process. In particular it is predicted that for a 0π pulse the spectral structure in the final population of both ρ_{22}^f and ρ_{33}^f has a periodicity which is twice that predicted for a hyperbolic-secant pulse envelope. This indicates that for a 0π pulse the direct two-photon transition dominates the accumulation process, while the one-photon sequential transitions are dominant for the hyperbolic-secant pulses. Also, it has been shown that, depending on the pulse shape and the kind of measurement that is performed, the atomic system response may be more or less sensitive to the frequency comb parameters Φ_R and T_R. A method is proposed for controlling the pulse repetition period T_R, independently of the interpulse phase Φ_R, which is important for optical metrology with femtosecond lasers. Further, we have analyzed the outcome of coherent-control experiments using pairs of pulses, including coherent-accumulation effects.

ACKNOWLEDGMENT

This work was supported by the Brazilian agencies CnPq and CAPES.

[1] A. H. Zewail, *Femtochemistry: Ultrafast Dynamics of the Chemical Bond* (Word Scientific, Singapore, 1994).
[2] S. A. Rice, Nature (London) **403**, 496 (2000).
[3] M. A. Bouchene, V. Blanchet, C. Nicole, N. Melikechi, B. Girard, H. Ruppe, S. Rutz, E. Schreiber, and L. Wöste, Eur. Phys. J. D **2**, 131 (1998).
[4] D. Meshulach and Y. Silberberg, Nature (London) **396**, 239 (1998).
[5] J. Degert, W. Wohlleben, B. Chatel, M. Motzkus, and B. Girard, Phys. Rev. Lett. **89**, 203003 (2002).
[6] N. Dudovich, D. Oron, and Y. Silberberg, Phys. Rev. Lett. **88**, 123004 (2002).
[7] J. E. Rothenberg, D. Grischkowsky, and A. C. Balant, Phys. Rev. Lett. **53**, 552 (1984).
[8] D. Felinto, C. A. C. Bosco, L. H. Acioli, and S. S. Vianna, Phys. Rev. A **64**, 063413 (2001).
[9] T. Udem, R. Holzwarth, and T. W. Hänsch, Nature (London) **416**, 233 (2002).
[10] S. T. Cundiff and J. Ye, Rev. Mod. Phys. **75**, 325 (2003).
[11] L. Hollberg, C. W. Oates, E. A. Curtis, E. N. Ivanov, S. A. Diddams, T. Udem, H. G. Robinson, J. C. Bergquist, R. J. Rafac, W. M. Itano, R. E. Drullinger, and D. J. Wineland, IEEE J. Quantum Electron. **37**, 1502 (2001).
[12] D. Felinto, C. A. C. Bosco, L. H. Acioli, and S. S. Vianna, Opt. Commun. **215**, 69 (2003).
[13] M. M. Salour, Rev. Mod. Phys. **50**, 667 (1978).
[14] J. N. Eckstein, A. I. Ferguson, and T. W. Hänsch, Phys. Rev. Lett. **40**, 847 (1978).
[15] M. J. Snadden, A. S. Bell, E. Riis, and A. I. Ferguson, Opt. Commun. **125**, 70 (1996).
[16] T. H. Yoon, A. Marian, J. L. Hall, and J. Ye, Phys. Rev. A **63**, 011402 (2000).
[17] L. Xu, C. Spielmann, A. Poppe, T. Brabec, F. Krausz, and T. W. Hänsch, Opt. Lett. **21**, 2008 (1996).
[18] D. Felinto, L. H. Acioli, and S. S. Vianna, Opt. Lett. **25**, 917 (2000).
[19] O. S. Heavens, J. Am. Oil Chem. Soc. **51**, 1058 (1961).
[20] H. Eicher, IEEE J. Quantum Electron. **11**, 121 (1975).
[21] W. H. Press, S. A. Teukolsky, W. T. Vetterling, and B. P. Flannery, *Numerical Recipes in C: The Art of Scientific Computing*

(Cambridge University Press, Cambridge, England, 1999).
[22] Y. Silberberg, V. L. da Silva, J. P. Heritage, E. W. Chase, and M. J. Andrejco, IEEE J. Quantum Electron. **28**, 2369 (1992).
[23] J. Mlynek, W. Lange, H. Harde, and H. Burggraf, Phys. Rev. A **24**, 1099 (1981).
[24] M. D. Crisp, Phys. Rev. A **1**, 1604 (1970).
[25] We remark that the mode structure of a femtosecond laser is usually expressed as $\omega_N = 2\pi N/T_R + \delta\omega$, where $\delta\omega$ is the frequency offset. This can be translated to our definitions by making $\omega_L + \Phi_R/T_R = \Delta\Psi/T_R \equiv \delta\omega$.